NEOPLASIA
www.neoplasia.com

Volume 13 Number 1 January 2011 pp. 49–59 49

Pleiotropic Stromal Effects of Vascular Endothelial Growth Factor Receptor 2 Antibody Therapy in Renal Cell Carcinoma Models[1]

Inga J. Duignan, Erik Corcoran, Anthony Pennello, Mary Jane Plym, Michael Amatulli, Nidia Claros, Michelle Iacolina, Hagop Youssoufian, Larry Witte, Selda Samakoglu, Jonathan Schwartz, David Surguladze and James R. Tonra

ImClone Systems, a wholly owned subsidiary of Eli Lilly and Company, New York, NY, USA

Abstract

The benefits of inhibiting vascular endothelial growth factor (VEGF) signaling in cancer patients are predominantly attributed to effects on tumor endothelial cells. Targeting non–endothelial stromal cells to further impact tumor cell growth and survival is being pursued through the inhibition of additional growth factor pathways important for the survival and/or proliferation of these cells. However, recent data suggest that VEGF receptor (VEGFR)–specific inhibitors may target lymphatic vessels and pericytes in addition to blood vessels. Here, in fact, we demonstrate that DC101 (40 mg/kg, thrice a week), an antibody specific to murine VEGFR2, significantly reduces all three of these stromal components in subcutaneous (SKRC-29) and orthotopic (786-O-LP) models of renal cell carcinoma (RCC) established in *nu/nu* athymic mice. Sunitinib (40 mg/kg, once daily), a receptor tyrosine kinase inhibitor of VEGFR2 and other growth factor receptors, also caused significant loss of tumor blood vessels in RCC models but had weaker effects than DC101 on pericytes and lymphatic vessels. In combination, sunitinib did not significantly add to the effects of DC101 on tumor blood vessels, lymphatic vessels, or pericytes. Nevertheless, sunitinib increased the effect of DC101 on tumor burden in the SKRC-29 model, perhaps related to its broader specificity. Our data have important implications for combination therapy design, supporting the conclusion that targeting VEGFR2 alone in RCC has the potential to have pleiotropic effects on tumor stroma.

Neoplasia (2011) 13, 49–59

Introduction

The vascular endothelial growth factor family consists of placental growth factor (PIGF), VEGF-A, VEGF-B, VEGF-C, and VEGF-D. These five ligands have overlapping yet distinct capacities to activate three VEGF receptors (VEGFR1, VEGFR2, and VEGFR3) [1,2]. In tumors, VEGF-C– and VEGF-D–mediated activation of VEGFR3 can initiate and maintain a network of lymphatic vessels [3], whereas it is mainly the VEGF-A (VEGF)–mediated activation of VEGFR2 that supports the development and maintenance of a tortuous, highly permeable blood vessel network [4]. Although clinical targeting of lymphatic vessels in cancer patients is at an early stage of development, the inhibition of VEGF-VEGFR2–mediated signaling has received extensive effort during recent decades after the discovery of VEGF [5].

The importance of VEGF-VEGFR2 signaling in cancer is most clearly highlighted by the therapeutic benefits of bevacizumab, a humanized antibody to VEGF, in colorectal [6,7], lung [8], renal [9], and breast [10] cancer patients. Interestingly, to date, approvals by regulatory agencies currently limit the use of bevacizumab to combination therapy, in part related to the minimal ability of bevacizumab monotherapy to regress tumors despite significant inhibition of measurable disease progression [11,12]. The benefits of combining bevacizumab with cytotoxic therapy in patients are associated with an increase in the maturational state of tumor blood vessels when VEGF-VEGFR2 signaling is inhibited [13]. In effect, VEGF-VEGFR2–targeted agents are thought to prune immature or nascent vessels that lack a pericyte coating and enrich for pericyte-coated mature vessels

Abbreviations: ANOVA, analysis of variance; RCC, renal cell carcinoma; TKI, receptor tyrosine kinase inhibitor; VEGF, vascular endothelial growth factor A

Address all correspondence to: James R. Tonra, PhD, ImClone Systems, a wholly owned subsidiary of Eli Lilly and Company, 450 E 29th St, New York, NY 10016.
E-mail: james.tonra@imclone.com

[1]Research was funded by ImClone Systems, a wholly owned subsidiary of Eli Lilly and Company.
Received 12 August 2010; Revised 7 October 2010; Accepted 9 October 2010

DOI 10.1593/neo.101162

[13–15]. Mature vessels are less leaky and would therefore contribute less toward the typically high interstitial pressure in tumors that limits the delivery of cytotoxic drugs to tumor cells [15–17].

The minimal ability of bevacizumab monotherapy to regress tumors by denying them a blood vessel network may be related to the inability of VEGF-VEGFR2–targeted agents to eliminate all tumor blood vessels [15–20]. This idea has led to combination efforts distinct from those using cytotoxic agents. VEGF-VEGFR2–targeted agents are being combined with therapies targeting additional signaling pathways that may directly or indirectly support endothelial cell survival in the face of VEGF-VEGFR2 blockade [21]. Alternatively, multitargeted small molecule receptor tyrosine kinase inhibitors (TKIs) that inhibit the activation of VEGFR2 and additional growth factor receptors are being used [14,17,19,22,23].

Pericytes surrounding mature tumor blood vessels reduce permeability [24] and provide mechanical support [25]. Pericytes also provide soluble factors [26] to endothelial cells possibly allowing for the survival of tumor endothelial cells during VEGF-VEGFR2 blockade. These supportive cells are generally not thought to express VEGFR2 [27,28], so other growth factor pathways, in particular platelet-derived growth factor (PDGF) receptor β (PDGFRβ), have been targeted in combination approaches aiming to eliminate pericytes to increase the susceptibility of endothelial cells forming mature blood vessels to VEGF-VEGFR2 inhibition [14,22,23]. For example, in subcutaneous xenograft models of pancreatic and non–small cell lung cancer, targeting PDGFRβ-positive pericytes increased the antivascular and antitumor effects of a rat antibody targeting murine VEGFR2, DC101 [21].

In contrast to bevacizumab, the small molecule TKI sunitinib that targets VEGFR1, VEGFR2, and VEGFR3, as well as PDGFRα and PDGFRβ, Kit, Flt-3, and CSF-1R [27], is approved as a single agent for the first-line treatment of metastatic renal cell carcinoma (RCC) with a clear cell histologic component [29]. Approximately 80% of sporadic RCC cases are of the clear cell or mixed clear cell type, with 57% of these patients having mutations in the von Hippel–Lindau (*vHL*) gene, and 98% of these patients exhibiting loss of heterozygosity [30–32]. Loss of vHL activity leads to constitutive activation of the hypoxia-inducible factor 1 (HIF-1), resulting in increased production of proangiogenic factors including VEGF [33]. Sunitinib not only inhibits tumor growth in systemic therapy–naive metastatic RCC patients with a clear cell histologic component but also significantly increases tumor regressions when compared with the cytokine therapy interferon α (31% *vs* 6% of patients) [34]. In a similar population of RCC patients, bevacizumab monotherapy was associated with tumor regression in only 13% of patients [35].

Mechanistically, it has been suggested that the ability to inhibit both VEGFR2 and PDGFRβ signaling may enhance the efficacy of sunitinib through increased antivascular effects compared with inhibitors specific for VEGF-VEGFR2, due to the targeting of pericytes [27,36]. However, VEGF and PlGF targeting with a soluble receptor construct (VEGF Trap) causes the loss of both normal tracheal capillaries and associated pericytes, with the pericytes thought to migrate away from the site of endothelial cell loss [37]. Furthermore, in a murine lung cancer model, VEGFR inhibition with soluble VEGFR2 delivered by adenovirus not only reduced tumor endothelial cells but also significantly reduced pericyte density [38]. Pericyte targeting in this model with a VEGF-targeted agent was thought to relate to reduced PDGFRβ activity downstream to the loss of endothelial cell–derived PDGF ligand. However, the demonstration of relatively low but detectable VEGFR2 expression by bovine retinal pericytes suggests the potential for a more direct effect [39].

The additional benefits of sunitinib in RCC patients compared with those achieved to date with bevacizumab monotherapy may therefore not be due to the targeting of PDGFRβ on pericytes but to the targeting of numerous pathways on endothelial, stromal and even tumor cells by this multitargeted TKI. The targeting of pericytes, as well as endothelial cells, may in fact only require the inhibition of VEGF signaling. However, the ability of VEGF-VEGFR2–targeted agents to reduce tumor pericytes in animal models has recently been shown to be model dependent [40], so this possibility needs to be examined specifically in RCC models.

In a separate area of tumor biology, VEGFR3 signaling is frequently associated with the induction of a lymphatic network in tumors that may contribute toward the metastasis of tumor cells to lymph nodes and distant organs [3,41]. Inhibiting both VEGFR2 and VEGFR3 may target both tumor lymphatic vessels and blood vessels and, in this way, increase the antitumor and antimetastatic effects of therapy [41]. However, in line with the potential for more pleiotropic stromal effects of agents targeting the VEGFR2 pathway alone than generally considered, targeting of this pathway has the potential to exert potent antilymphatic effects [42]. In particular, VEGFR2 activation supports lymphangiogenesis into a collagen scaffold covering a circumferential area of mouse tail from which a band of dermal tissue was removed [42]. In addition, VEGFR2 blockade with DC101 prevents lymphatic vessel formation in regenerated mouse back skin after punch biopsy [43]. These findings indicate that targeting VEGFR2 alone has the potential to inhibit tumor lymphangiogenesis and its associated lymphatic metastasis.

From these discussions, it is clear that stromal cell effects of VEGFR2 inhibition in RCC tumors may not be limited to endothelial cells. In this regard, we have evaluated the effects of specifically targeting VEGFR2 with DC101 on tumor blood vessels, pericytes, and lymphatic vessels in two vHL-deficient RCC models. In addition, we have compared the effects of DC101 with those of the multitargeted TKI sunitinib, alone or in combination.

Materials and Methods

Cell Lines

Caki-1 and ACHN cells were both obtained from American Type Culture Collection (ATCC, Manassas, VA). The human clear cell RCC cell line 786-O was obtained from ATCC, and 786-O cells expressing firefly luciferase (786-O-LP) were generated by retroviral transfection, as previously described [44]. SKRC-29 RCC cells were obtained from Cornell Medical Center (New York, NY) [45]. Cells were cultured at 37°C/5% CO_2 in RPMI 1640 + 0.8 mg/ml geneticin (786-O and 786-O-LP), minimum essential medium (SKRC-29 and ACHN), or McCoy's 5A (Caki-1; Invitrogen Corporation, Carlsbad, CA), supplemented with 10% fetal bovine serum (HyClone, Lenexa, KY) and 1% GlutaMAX (Invitrogen Corporation). Cells were passaged or collected for injection into mice using Trypsin EDTA (Invitrogen Corporation).

vHL Gene Sequencing

Genomic DNA was extracted from cultured cells using the Qiagen QiaAmp DNA mini kit (Valencia, CA). Exons 1, 2, and 3 of *vHL* were

amplified from genomic DNA using Platinum HiFi PCR Supermix (Invitrogen Corporation) and the following primer sets:

Exon 1, 5′-TGGGTCGGGCCTAAGCGCCGGGCCCGT-3′, 5′-AGTGGAAATACAGTAACGAGTTGGCCT-3′
Exon 2, 5′-CTTTAACAACCTTTGCTTGTCCCGATA-3′, 5′-GTCTATCCTGTACTTACCACAACACCT-3′
Exon 3, 5′-CTGAGACCCTAGTCTGCCACTGAGGAT-3′, 5′-CAAAAGCTGAGATGAAACAGTGTAAGT-3′

Reactions were carried out using a Px2 Thermal Cycler (Thermo Scientific, Waltham, MA). Polymerase chain reactions were purified from a 1.2% Agarose TAE gel using a Qiagen Qiaquick Gel Extraction Kit. Purified products were then sequenced using the amplification primers above or an additional set of primers in the case of the *vHL* exon 1:

5′GCGGCGTCCGGCCCGGGTGGTCTGGAT-3′ and 5′-GACTGCGATTGCAGAAGATGACCTGGG-3′.

Sequencing was performed on an ABI Prism 3700 DNA Analyzer (Applied Biosystems, Foster City, CA) and analyzed using Vector NTI Advance 10 software (Invitrogen Corporation).

Western Blot

Cells were grown to 80% confluence in complete medium, and then culture supernatants were collected and cells were lysed with radioimmunoprecipitation assay buffer (Santa Cruz Biotechnology, Santa Cruz, CA). The protein concentration in cell lysates was measured using bicinchoninic acid (Pierce, Rockford, IL). Lysates (40 μg protein/lane) were run on a 4% to 12% NuPAGE gel (Invitrogen Corporation), transferred to nitrocellulose, and stained with primary antibodies for *vHL* (Cell Signaling Technology, Inc, Denver, MA) and β-actin (Sigma-Aldrich, St Louis, MO). Enhanced chemiluminescence (Amersham, Piscataway, NJ) was used to develop images on an LAS-4000 luminescent image analyzer (Fujifilm Life Sciences, Stamford, CT).

Mice

Female *nu/nu* athymic mice (6-8 weeks old at study initiation; Charles River Laboratories, Wilmington, MA) were used in accordance with current regulations and standards of the US Department of Agriculture and the National Institutes of Health, with all animal research methods approved by an internal animal care and use committee.

Orthotopic 786-O-LP Tumor Model

A longitudinal incision was made approximately 10 to 12 mm lateral to the spine on the dorsal surface, directly above the kidney, in isoflurane-anesthetized mice. The left kidney was isolated under the abdominal muscle layer and grasped with blunt tipped forceps. The kidney was moved to the site of incision, and 3×10^6 786-O-LP cells were injected just below the renal capsule in 100% Matrigel (BD Biosciences, San Jose, CA), in a 50-μl volume using a 30-gauge needle. The kidney was returned to the peritoneal cavity, and the surgical site was closed first by suturing the abdominal wall with 4-0 silk sutures and then by closing the skin with wound clips. Tumor burden was evaluated in live animals by measuring bioluminescence intensity (BLI) using the IVIS 200 *in vivo* imaging system, as per the manufacturer's instructions (Xenogen/Caliper Life Sciences, Hopkinton, MA). BLI was evaluated 12 minutes after intraperitoneal injection of 150 mg/kg D-luciferin (Xenogen), as previously described [44]. Ten days after tumor cell injection, mice were randomized by BLI into treatment groups, and BLI was evaluated during the treatment period. Furthermore, at the end of dosing in studies evaluating the antitumor effects of treatment, tumor burden was evaluated by measuring the weight of the injected kidney. Effects of treatment on bioluminescence signal ($\log_{10}$[BLI]) over time were evaluated by repeated-measures analysis of variance (ANOVA; n = 10-11 mice per group; JMP version 5; SAS, Cary, NC). The effects of treatment on tumor-bearing kidney weight were evaluated by one-way ANOVA followed by Fisher least significant difference (LSD; n = 10-11 mice per group; SigmaStat, Point Richmond, CA).

SKRC-29 Subcutaneous Xenograft Tumor Model

Mice were injected subcutaneously into the right flank with 2×10^6 SKRC-29 cells, in 50% culture medium/50% Matrigel. Tumor volumes were calculated as $\pi/2(L \times W^2)$, where L is the longest diameter measured with calipers and W is the diameter perpendicular to L. When the mean tumor volume reached approximately 250 mm^3, mice were randomized by tumor volume into treatment groups and tumor volume was recorded twice weekly thereafter. The effects of treatment on tumor growth were evaluated by repeated-measures ANOVA (n = 11-12 mice per group).

Treatments

DC101 (ImClone Systems, Branchburg, NJ) was diluted in USP saline (Braun Medical, Inc, Irvine, CA) and dosed Monday-Wednesday-Friday at 40-mg/kg body weight. Sunitinib (Sequoia Research Products, Pangbourne, UK) was prepared in 0.5% methyl cellulose (Sigma-Aldrich) with 0.2% Tween 80 (Sigma-Aldrich), and dosed by oral gavage at 40 mg/kg, once a day. All treatments were started on the same day. When dosed in combination, on days in which both drugs were administered, sunitinib was administered approximately 1 hour before DC101.

Thin-Section Immunohistochemical Analysis

SKRC-29 tumors were removed 7 days after the start of treatment, fixed in 10% neutral-buffered formalin at 4°C for 24 hours, and then embedded in paraffin. Five μm sections were double-stained with monoclonal antibodies for CD31 (Gene Tex, Irvine, CA) and alpha-smooth muscle actin (αSMA; Epitomics, Burlingame, CA), using Alexa Fluor 488 (Molecular Probes, Eugene, OR) and tetramethyl rhodamine iso-thiocyanate (BioFX, Owings Mills, MD) to fluorescently detect the proteins, respectively. In addition, thin sections of saline-treated SKRC-29 tumors, as well as 786-O-LP tumors, were stained for CD31/αSMA/VEGFR2 and CD31/LYVE-1/VEGFR2 using the antibodies described above and a monoclonal antibody to VEGFR2 (Abcam, Cambridge, MA) and/or a rabbit polyclonal antibody to LYVE-1 (Novus Biologicals, Littleton, CO). CD31, αSMA, and LYVE-1 were visualized with Alexa Flour 488 or TRITC in these sections, and VEGFR2 was visualized with Alexa Fluor 647 (Molecular Probes).

Fluorescent images of thin sections at 400× magnification were captured using EZ-C1 software with a Nikon C1 confocal microscope (Nikon Instruments, Inc, Melville, NY). Quantitative analyses of CD31/αSMA–stained sections were performed on images from five fields of view from the tumor periphery (within 0.44 mm^2 from the tumor edge) and five from the tumor core (>0.5 mm^2 from the tumor edge). After finding no effect of tumor location (not shown),

these measurements were pooled for a total of 10 fields of view per tumor. NIS Elements software (Nikon Instruments, Inc) was used for the quantification of total positive signal area in the captured fields of view, expressed as a percentage of total field of view area. Treatment effects on histologic measurements were evaluated by one-way ANOVA, followed by Fisher LSD (n = 6 tumors per group).

Thick-Section Histologic Analysis

SKRC-29 tumors and 786-O-LP tumor-bearing kidneys were removed 7 days after the start of treatment and placed in 4% paraformaldehyde (EM Sciences, Hatfield, PA) for 1 hour. Tissues were then placed in 1% paraformaldehyde on ice until 200-μm sections were cut with a vibrating blade microtome (VT1000S; Leica, Bannockburn, IL) and placed in Lab-Tek chamber slides (Nunc, Rochester, NY). Sections were stained with primary antibodies for CD31 (Gene Tex), αSMA (Epitomics), type IV collagen (Millipore, Billerica, MA), NG2 (Millipore), LYVE-1 (Novus Biologicals), and/or mouse pan-endothelial cell antigen (Meca-32; BD Pharmingen, Franklin Lakes, NJ). For fluorescent detection, an Alexa Fluor 488–conjugated secondary antibody was used for CD-31 (Molecular Probes), and a TRITC-conjugated antibody was used for αSMA and LYVE-1 (BioFX). Meca-32 and NG2 were visualized using Alexa Fluor 647, and type IV collagen was visualized with Alexa Fluor 633 (Molecular Probes). CD31 staining was used for evaluating treatment effects on blood vessels throughout, given that nearly all CD31-positive vessels were also Meca-32–positive (not shown).

For the analysis of treatment effects on SKRC-29 tumors, the following triple stains were performed: CD31/αSMA/type IV collagen, CD31/αSMA/NG2, and CD31/LYVE-1/type IV collagen (n = 3 tumors per treatment group). In 786-O-LP tumors, the following triple stains were performed: CD31/αSMA/type IV collagen and CD31/LYVE-1/Meca-32 (n = 6 tumors per group). Images were acquired using EZ-C1 software on a Nikon C1 confocal microscope. A total of 10 Z-stacks were captured per stained tissue section. Selection of the fields of view for analysis involved randomly selecting hot spots for αSMA staining in the SKRC-29 model. Hot spots of αSMA staining were again part of the selection criteria in the 786-O-LP model, but selected areas were also required to be in the tumor cell–rich regions and distinct from normal regions of the adjacent kidney dominated by tubular structures and/or glomeruli.

For the evaluation of SKRC-29 tumors, because the effect of treatment on type IV collagen and NG2-positive structures staining was minimal (not shown), the analysis of CD31 and αSMA staining from the CD31/αSMA/type IV collagen and CD31/αSMA/NG2 triple-stained sections was pooled, making for a total of 20 Z-stacks analyzed per tumor. The quantification of effects of treatment on tumor stroma included the counting of all individual vessel like structures in one plane in the middle of each captured Z-stack using AutoQuant software (Media Cybernetics, Inc, Acton, MA) and the characterization of these structures as a single or a double positive for CD31 and αSMA (n = 3 tumors per group). The same analysis was performed to evaluate LYVE-1–positive vessel-like structures in the SKRC-29 model. In addition to the vessel counting method, the total volume of CD31- and αSMA-stained pixels throughout all CD31/αSMA/type IV collagen– and CD31/αSMA/NG2–stained Z-stacks was measured with NIS Elements software. The results using this last method were very similar to those obtained using the manual counting method described above, so only the NIS Elements method was used in the 786-O-LP–stained tumors for CD31, αSMA, and LYVE-1 analyses (n = 6 tumors per group). The effects of treatment on quantitative measures of immunostaining were evaluated by one-way ANOVA followed by Fisher LSD, with n always taken as the number of tumors per treatment group.

Results

SKRC-29 Subcutaneous Tumor Model

The SKRC-29 cells used in these studies have an early stop codon in the *vHL* gene because of a C203A base pair mutation, causing a lack of vHL protein expression compared with *vHL* wild type RCC cells (Figure 1). Thus, SKRC-29 cells exhibit a major characteristic of clear cell RCC [17,30,32], although, at the time of isolation of this cell line from a patient, the characterization of the histology of the tumor was not reported [45]. SKRC-29 cells formed rapidly growing tumors when implanted subcutaneously into athymic *nu/nu* mice (Figure 2*A*).

An antibody to mouse VEGFR2, DC101, and a TKI of VEGFR2, sunitinib, had similar and potent antitumor effects in the SKRC-29 subcutaneous xenograft RCC model (P < .001; Figure 2*A*). Interestingly, although both agents target VEGFR2, the combination of sunitinib and DC101 resulted in a greater inhibition of tumor growth than either monotherapy (P < .02). Furthermore, tumors in 6 of 11 mice in the DC101 + sunitinib group decreased in volume during 26 days of therapy compared with 1 of 12 and 1 of 11 in the DC101 and sunitinib monotherapy groups, respectively (P = .002 for an effect of treatment by χ^2 test).

To examine the mechanisms underlying the efficacy illustrated in Figure 2*A*, SKRC-29 tumors were harvested after 7 days of therapy for the analysis of the density of CD31-positive blood vessels, LYVE-1–positive lymphatic vessels [42] and α-smooth muscle actin (αSMA)–positive pericytes [14,17,21,46]. This time point was selected because tumors in all treatment groups were still of similar size, and significant blood vessel loss occurs in animal models by 7 days of VEGFR2-targeted therapy [17,20].

In thick sections (200 μM) of tumors stained for both CD31 and αSMA, it was rare to find CD31-positive vessel-like structures consisting of one or more continuous linear segments not associated with αSMA-positive pericytes (Figure 3, *A* and *B*). In contrast, numerous vessel-like structures positive for αSMA only, or CD31-positive endothelial cells in association with αSMA-positive structures were observed. Sunitinib significantly reduced the density of αSMA/CD31 double-stained vessels (P < .05), frequently referred to as mature or established vessels [14,21]. In contrast, sunitinib increased the

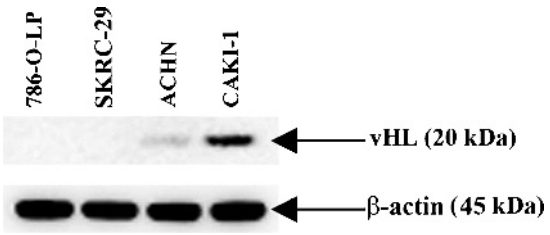

Figure 1. *vHL* mutant RCC lines lack vHL protein expression. Forty micrograms of total lysate protein per lane from the indicated cell lines was run on a 4% to 12% NuPAGE gel. After transfer to nitrocellulose, blots were stained for vHL and β-actin (loading control).

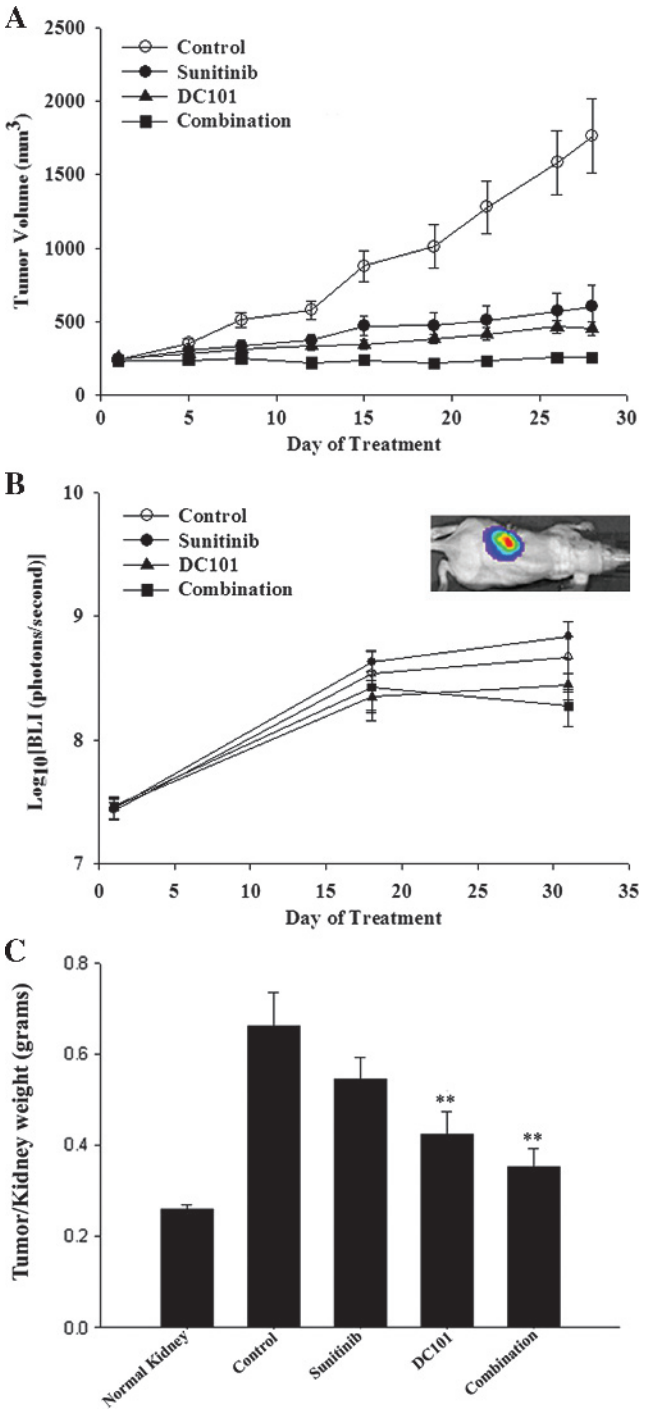

Figure 2. Targeting VEGFR2 significantly inhibits xenograft tumor growth in RCC models. (A) DC101 (40 mg/kg, intraperitoneally, Monday-Wednesday-Friday) and sunitinib (40 mg/kg, per os, once daily), alone or in combination, significantly decreased the growth of established subcutaneous SKRC-29 tumors in *nu/nu* athymic mice. (B) Treatments, as described in panel A, did not significantly impact the change in bioluminescence signal over time, emitted from 786-O-LP cells growing in the kidney. Inset illustrates bioluminescence image on IVIS 200, with red indicating regions of greatest signal and purple indicating regions of lowest detectable signal. (C) DC101 alone or in combination with sunitinib, but not sunitinib alone, significantly decreased the weight of 786-O-LP tumor-bearing kidneys harvested after 32 days of treatment. $^{**}P < .01$ *versus* control = saline treatment. All graphs plot mean ± SEM.

frequency of vessel-like structures staining positively for αSMA only ($P < .05$) but did not affect the total number of αSMA structures. This suggests sunitinib depletes CD31-positive endothelial cells, without affecting the pericytes that were supporting these lost vessels, as previously reported [17]. This is in contrast to DC101, which depleted both total CD31-positive and total αSMA-positive vessel-like structures ($P < .05$), but did not affect the density of αSMA-only structures (Figure 3, *A* and *B*). DC101 therefore seems to be targeting both CD31-expressing blood vessels as well as the pericytes that support these vessels. In combination, the histologic effects of DC101 + sunitinib were not significantly different from those of DC101 alone (Figure 3, *A* and *B*).

It was somewhat unexpected that a more specific VEGFR2-targeting agent (DC101) reduced pericytes to a greater extent than a potent VEGFR2-targeted agent that also targets PDGFRβ [21,27]. Additional quantitative methods were therefore performed to confirm the results presented in Figure 3, *A* and *B*. First, total CD31- and total αSMA-positive volumes were summed separately through the entire captured image stacks from thick sections, with a computerized process that is much less time-consuming than counting individual vessels (Figure 3*C*). Results of this volume quantification were very similar to those obtained by counting and characterizing individual structures in tumor sections, with both DC101 and sunitinib, alone or in combination, reducing CD31 staining volume ($P < .05$), but only DC101 significantly reducing αSMA staining volume (Figure 3*C*). The effects of DC101 + sunitinib combination therapy on CD31 and αSMA staining volume were not significantly different from those of DC101 alone.

As an additional quantitative method, we evaluated the effects of treatment in thin sections of formalin-fixed paraffin-embedded tumors using methods more frequently used in evaluating the effects of antivascular agents in xenograft models [17,20,21]. As with thick-section analyses, sunitinib and DC101, alone or in combination, had similar potency in reducing the area of CD31-expressing tumor blood vessels ($P < .05$; Figure 3*D*). Moreover, DC101 had a dramatic effect on the total αSMA-positive area ($P < .05$), whereas the trend for an effect of sunitinib did not reach statistical significance (Figure 3*D*). It is noteworthy that the density of αSMA staining relative to CD31 was much lower in thin sections of formalin-fixed paraffin-embedded tissue compared with thick sections that undergo relatively minimal fixation and tissue processing before staining (Figure 3, *C* and *D*). This difference may indicate improved αSMA staining sensitivity or better preservation of αSMA-positive structures with the thick-section methods used.

786-O-LP Orthotopic Tumor Model

To examine the generality of the findings in the SKRC-29 subcutaneous xenograft tumor model, we used a luciferase-expressing clear cell RCC line, 786-O-LP (for parental line, see Gnarra et al. [30]). The *vHL* gene in this line also possesses genetic changes (G311 deletion) associated with a lack of vHL protein expression (Figure 1). 786-O-LP tumor cells were surgically implanted just under the renal capsule of mice. DC101 and DC101 + sunitinib both tended to reduce the BLI emitted from the tumor growing within live mice up to the point of study termination, but the effect did not reach statistical significance (Figure 2*B*). As a measure of total tumor burden, we also recorded the weight of the tumor-bearing kidneys at the end of the study (Figure 2*C*). The weight of the non–tumor-bearing kidney from the control group mice was also recorded as a measure of normal kidney weight. DC101 and DC101 + sunitinib both significantly

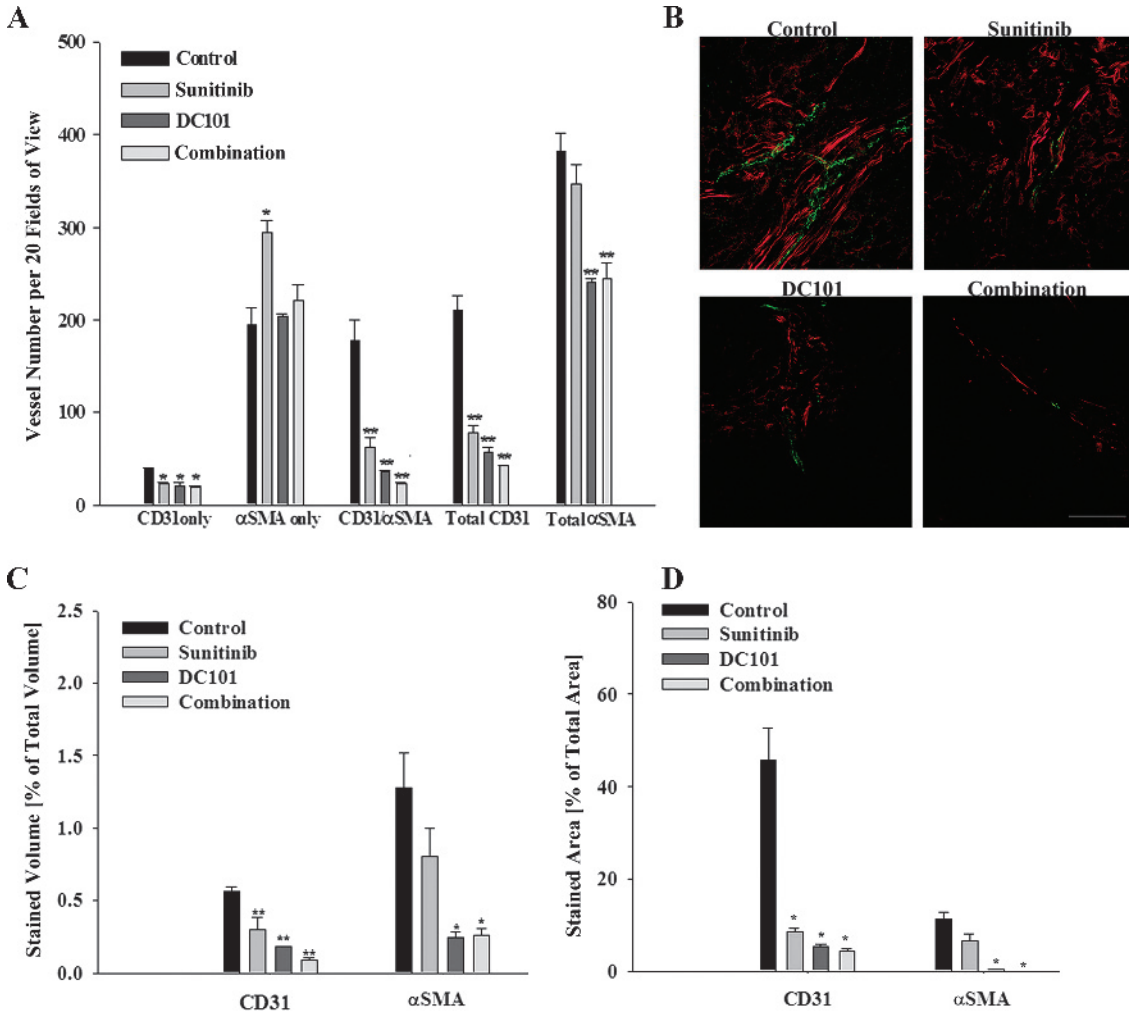

Figure 3. DC101 targets blood vessels and pericytes in subcutaneous SKRC-29 RCC tumors. (A) Two hundred-micrometer-thick sections of SKRC-29 subcutaneous xenograft tumors grown in *nu/nu* athymic mice were immunostained for CD31 and αSMA. Tumors were harvested after 7 days of treatment with DC101 (40 mg/kg, intraperitoneally, Monday-Wednesday-Friday) and sunitinib (40 mg/kg, per os, once daily), alone or in combination. All treatments significantly reduced CD31-positive vessels, but only DC101 and DC101 + sunitinib reduced total αSMA staining. (B) Representative images for the analysis reported in panel A, with red = αSMA and green = CD31-positive fluorescence. Bars, 20 μm. (C) Volume of positive staining calculated with NIS Elements software is reported for the same three-dimensional image stacks used for the counting of individual structures in panel A, with similar effects of treatment. (D) Five-micrometer-thin sections of formalin-fixed paraffin-embedded tumors, harvested after 7 days of treatment with DC101 and sunitinib, alone or in combination, were stained for CD31 and αSMA. As above, all treatments significantly reduced CD31-positive vessels, but only DC101 and DC101 + sunitinib reduced total αSMA staining. All graphs plot mean ± SEM. *$P < .05$ *versus* control = saline treatment; **$P < .01$ *versus* control.

reduced the weight of the tumor-bearing kidney ($P < .004$) with similar potency ($P = .37$), but the effects of sunitinib monotherapy did not reach statistical significance *versus* control ($P = .14$). Of note for the kidney contralateral to the kidney injected with tumor cells, no tumor cells were observed by whole body bioluminescence imaging and no abnormalities were visualized at sacrifice in any treatment group.

To study the mechanisms underlying the treatment effects illustrated in Figure 2, *B* and *C*, 786-O-LP tumors were harvested after 7 days of therapy for the analysis of the volume of CD31- and αSMA-positive staining, in thick sections only. Both DC101 and sunitinib significantly reduced CD31 staining, with DC101 having a greater effect ($P < .05$; Figure 4, *A* and *B*). Similarly, DC101 reduced the volume of αSMA staining by 60% ($P < .05$), whereas sunitinib reduced this pericyte-associated staining by only 23% ($P < .05$). For both CD31 and αSMA, the effects of combination therapy with DC101 + sunitinib were not significantly different from those of DC101 alone.

Treatment Effects on Tumor Lymphatic Vessels

LYVE-1 staining density was evaluated in tumor sections to examine the effects of targeting VEGFR2 on lymphatic vessels [42]. In thick sections of SKRC-29 subcutaneous tumors, DC101 significantly reduced lymphatic vessel density ($P < .05$), whereas sunitinib did not (Figure 5, *A* and *B*). The combination DC101 + sunitinib had an effect similar to that of DC101 alone. In volumetric quantification of LYVE-1 staining in thick sections of 786-O-LP orthotopic tumors,

both DC101 and sunitinib reduced lymphatic vessel density, with DC101 having a greater effect than sunitinib ($P < .05$) and the combination therapy having an effect similar to that of DC101 alone (Figure 5, *C* and *D*).

Colocalization of VEGFR2 with CD31, LYVE-1, and αSMA

Whereas the effects of a VEGFR2-specific agent such as DC101 on lymphatic endothelial cells and pericytes may be indirect and potentially downstream to the effects on endothelial cells, a more direct effect is possible [39,43]. A direct effect would require VEGFR2 expression by lymphatic endothelial cells and pericytes, so we evaluated the colocalization of VEGFR2 immunoreactivity with LYVE-1–positive lymphatic vessels and αSMA-positive pericytes in sections of tumors from control mice. As expected, CD31-positive endothelial cells were VEGFR2-immunoreactive in the SKRC-29 and 786-O-LP models (Figure 6, *A* and *B*). VEGFR2 immunoreactivity also colocalized with αSMA-positive (Figure 6, *C* and *D*) and LYVE-1–positive (Figure 6, *E* and *F*) structures, supporting VEGFR2 expression by pericytes and lymphatic endothelial cells in these models.

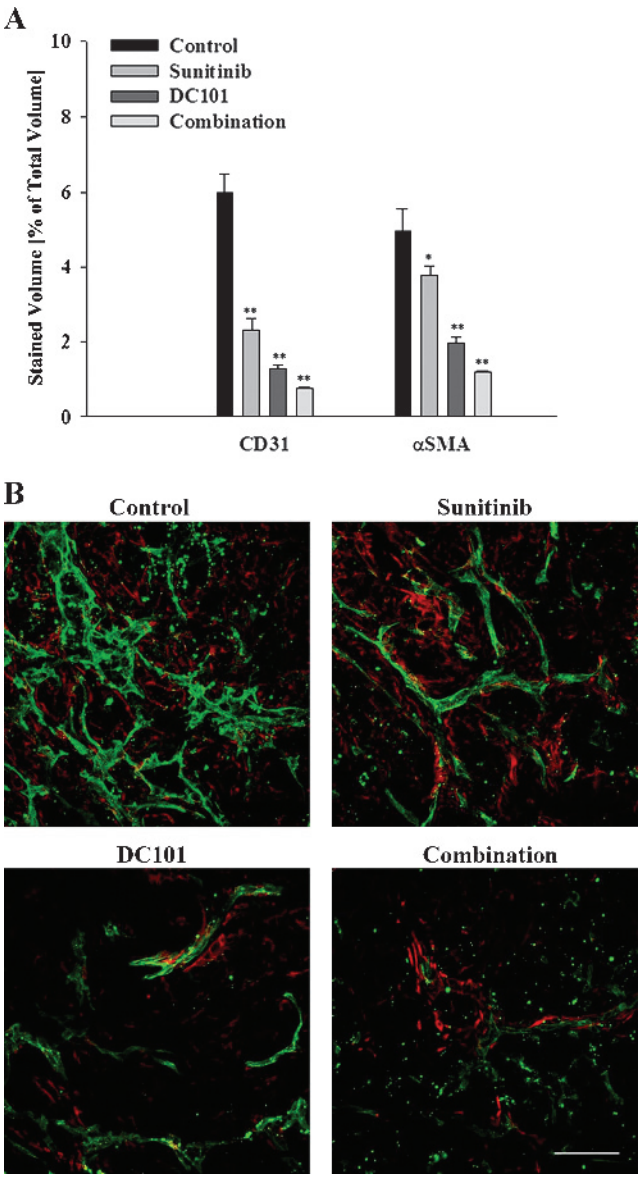

Figure 4. DC101 targets blood vessels and pericytes in orthotopic 786-O-LP RCC tumors. (A) Two hundred-micrometer-thick sections of 786-O-LP tumor-bearing kidneys were immunostained for CD31 and αSMA. Tissues were harvested after 7 days of treatment with DC101 (40 mg/kg, intraperitoneally, Monday-Wednesday-Friday) and sunitinib (40 mg/kg, per os, once daily), alone or in combination. All treatments significantly reduced the volume of CD31-positive and αSMA-positive staining, with DC101-containing regimens having the greatest effect. *$P < .05$ *versus* control = saline treatment; **$P < .01$ *versus* control. Mean ± SEM is plotted. (B) Representative images for the analysis reported in panel A, with red = αSMA and green = CD31-positive fluorescence. Bar, 20 μm.

Discussion

The genetic diversity of cancer cells and the biologic complexity of tumor growth underlie a significant current effort to develop combination therapies targeting multiple pathways. We recently demonstrated that two characteristics associated with the best combination of targeted agents were inhibition of resistance mechanisms of one agent in the combination by another agent and a nonoverlapping spectrum of activity [47]. This last factor was related to the finding that targeting one pathway obviated the need to target a separate pathway in the models tested, despite the fact that both agents had antitumor effects on their own. Here, we demonstrate another of these instances, where an agent specifically targeting VEGFR2 was found to have effects on the tumor stroma frequently thought to be achievable only by adding agents targeting different pathways in a combination approach. More specifically, an antibody targeting VEGFR2 not only dramatically reduced tumor blood vessel density in vHL-deficient RCC models as expected but also reduced the density of tumor pericytes and lymphatic vessels.

The importance of VEGF-VEGFR2 signaling in endothelial cell functioning within tumors is well established. Early in the first week of treatment with VEGF-VEGFR2–specific agents in preclinical cancer models, the large-diameter, highly permeable, and tortuous tumor blood vessel networks are normalized, in that blood vessels lose more than 85% of their endothelial cell fenestrations after only 1 day of treatment [19], and vessel diameter is decreased within 2 days [18]. Related to increased vessel permeability, the typically high interstitial fluid pressure within the tumor [48] is significantly reduced within 3 days of DC101 treatment [46]. This effect likely underlies the reported increase in the delivery of blood-borne compounds to tumors during VEGF-VEGFR2–targeted therapy [15,17,46]. Furthermore, this window of increased drug access may contribute toward the demonstrated therapeutic benefits of an antibody to VEGF, bevacizumab, in combination with cytotoxic therapy in patients [6–8,10,15].

After 1 week of VEGF-VEGFR2–targeted therapy, following this period of more normal vessel functioning, tumor blood vessels as well as some blood vessels in normal tissue are lost [18–20,49]. But in all cases, a small population of tumor blood vessels survive, likely contributing to the finding that tumors do not significantly regress with VEGF-VEGFR2–specific agents [20,49,50]. The remaining vessels are often considered to be the more mature pretreatment vessels that survived specific VEGF-VEGFR2–targeted therapy through a supply of additional trophic support from pericytes [14,21,46]. Targeting of the remaining vessels has therefore emerged as a potential combination approach, supported by the finding that targeting PDGFRβ, a receptor important for the survival and functioning of pericytes, in addition to targeting VEGF-VEGFR2 signaling, can increase vessel loss and antitumor effects in models of pancreatic islet cell cancer [14], pancreatic cancer, and non–small cell lung cancer [21].

Yet here we show in tumor models with an impaired ability to downregulate HIF-1 activity, a commonly observed deficiency in clear cell RCC, that targeting VEGFR2 alone with a specific monoclonal antibody causes the loss of tumor blood vessels as well as their associated αSMA-positive pericytes. Surprisingly, the magnitude of the effect of an antibody specific to VEGFR2 on pericytes was greater than that achieved with a small molecule TKI that potently inhibits both VEGFR2 and PDGFRβ [27]. The dose of sunitinib used in the current studies (40 mg/kg, PO, once daily) is the most frequently used dose in the literature because of its maximal antitumor effect [23,27] and significant antivascular effect [17]. However, this dose inhibited VEGFR2 phosphorylation in tumors at 12 but not 24 hours after treatment, whereas a higher dose (80 mg/kg) inhibited PDGFRβ phosphorylation at both time points [27]. It is therefore possible that a higher dose of sunitinib would achieve the same magnitude of effect as DC101 on tumor pericytes observed in the present studies. Nevertheless, the modest effect of 40 mg/kg sunitinib in the 786-O-LP model (23% decrease in αSMA-positive pericyte staining) is consistent with a reported 33% decrease in αSMA-positive pericytes in tumors treated with AG013736 [19], a TKI targeting VEGFRs, PDGFRs, and cKit. Moreover, the absence of an effect on tumor αSMA-positive pericytes in the presence of a significant antivascular effect after 7 days of treatment with sunitinib in the SKRC-29 model is very similar to results reported in a glioma model [17]. Regardless

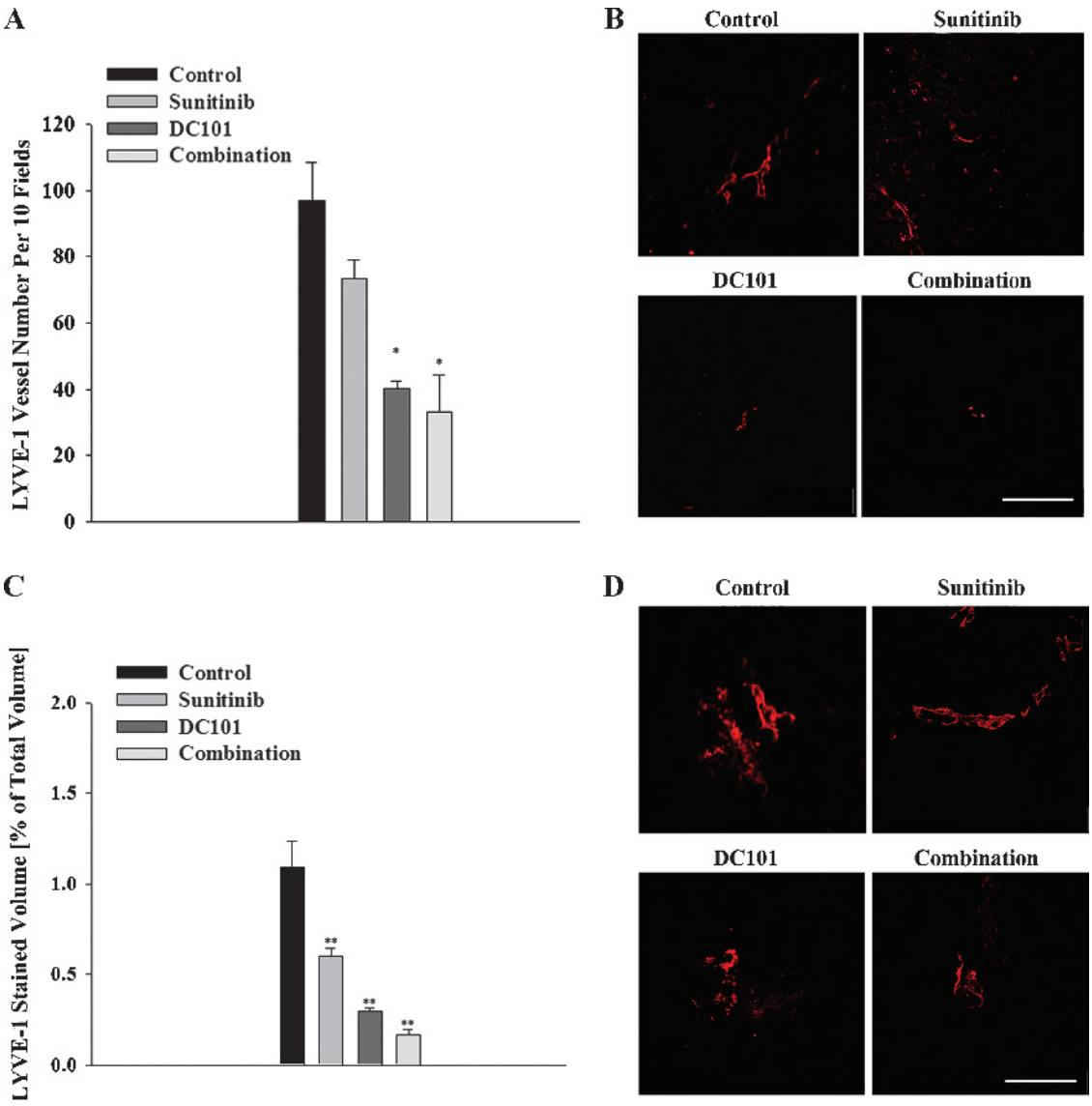

Figure 5. DC101 targets lymphatic vessels in RCC tumors. (A) SKRC-29 subcutaneous tumors were harvested after 7 days of treatment with DC101 (40 mg/kg, intraperitoneally, Monday-Wednesday-Friday) and sunitinib (40 mg/kg, per os, once daily), alone or in combination, and 200-μm-thick sections were stained for LYVE-1. Only DC101 and DC101 + sunitinib reduced total LYVE-1–positive lymphatic vessel density. (B) Representative photomicrographs of LYVE-1–immunostained tumor sections with red = LYVE-1–positive fluorescence for panel A. (C) 786-O-LP orthotopic tumors were harvested after 7 days of treatment as above, and 200-μm-thick sections were stained for LYVE-1. DC101 and sunitinib both reduced total LYVE-1–positive stained volume, calculated using NIS Elements software, with DC101 having a greater magnitude effect. (D) Representative images of LYVE-1–immunostained tumor sections with red = LYVE-1–positive fluorescence for panel C. All graphs plot mean ± SEM. Bars, 20 μm. *$P < .05$ *versus* control = saline treatment; **$P < .01$ *versus* control.

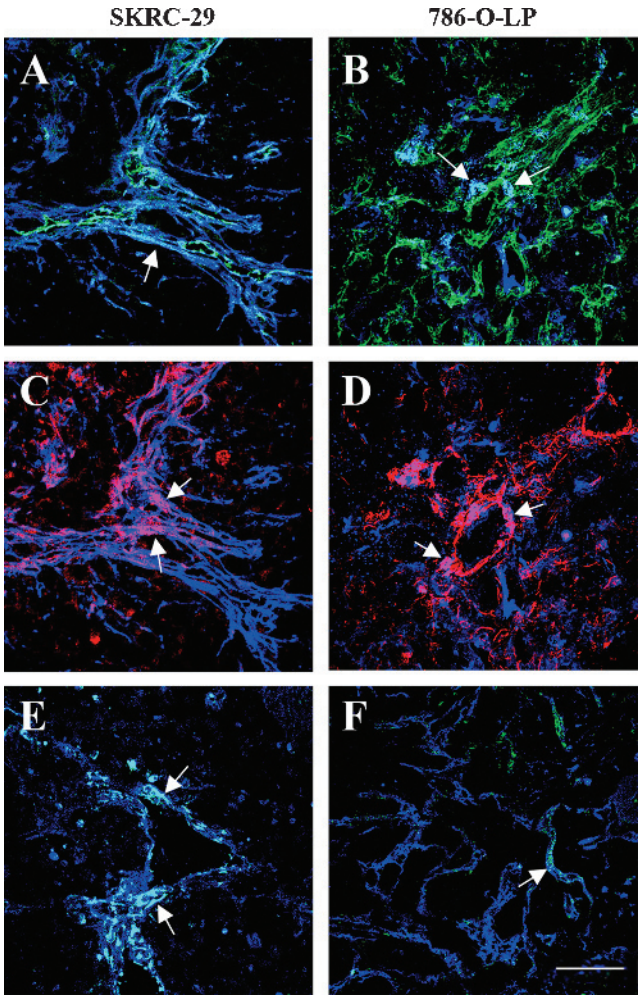

Figure 6. VEGFR2 colocalizes with CD31, LYVE-1 and αSMA in RCC tumors. Representative images are shown for VEGFR2 immunostaining (blue fluorescence) of 5-μm-thin sections of formalin-fixed paraffin-embedded SKRC-29 (A, C, and E) and 786-O-LP (B, D, F) tumors from control = saline-treated mice, double-stained for CD31 (green in A and B), αSMA (red in C and D), and LYVE-1 (green in E and F). Arrows indicate colocalization of fluorescence for VEGFR2 and CD31 (light blue in A and B), VEGFR2 and αSMA (pink in C and D), and VEGFR2 and LYVE-1 (light blue in E and F). Bars, 20 μm.

of the effects of TKIs, however, results with DC101 clearly show that targeting blood vessel–associated pericytes does not require the targeting of a receptor other than VEGFR2 in renal cell cancer models.

Combination approaches seeking to add to the benefits of VEGF-VEGFR2 pathway–targeted agents may also include the targeting of lymphatic endothelial cells by inhibiting pathways important for lymphangiogenesis such as VEGFR3 [41]. This combination strategy aims to limit the lymphatic spread of metastasis while also inhibiting angiogenesis-dependent components of cancer progression. Yet, in two RCC models, a significant depletion of tumor lymphatic vessels was achieved by targeting VEGFR2 alone with DC101. This finding is in agreement with the reported effects of targeting VEGFR2 on lymphangiogenesis after skin damage in animal models [42,43]. Although the effects of DC101 on tumor pericytes and lymphatic endothelial cells may be indirect [37,38], the immunohistochemical colocalization of VEGFR2 and LYVE-1, as well as VEGFR2 and αSMA, supports the possibility that targeting may also be direct [39,43].

The pleiotropic effects of VEGFR2-targeted therapy on tumor stroma were consistent in models established with two different cell lines in two different tissue environments; however, the impact of these effects on tumor burden was weaker in the orthotopic 786-O-LP model than in the subcutaneous SKRC-29 model. We have not compared the antitumor effects of treatment in both environments in models established with the same cell line; however, the effects of sunitinib at the 40-mg/kg dose level have recently been evaluated in a subcutaneous tumor model established with the parental line for 786-O-LP, 786-O [51]. Sunitinib caused tumor stasis in this subcutaneous model, in contrast to the lack of effect reported here when 786-O-LP cells were grown orthotopically. This suggests that the differences in efficacy may be due to environmental factors, with the kidney environment allowing for tumor growth despite significant antivascular effects. Nevertheless, a definitive conclusion cannot be made without using the same cell lines in the two model systems.

In summary, results indicate that targeting VEGFR2 with an antibody in vHL-deficient RCC may obviate the need for other agents specifically targeting pericytes and lymphatic vessels to increase antitumor effects. This conclusion is highlighted by the finding that combining DC101 with a TKI that inhibits VEGFR2, VEGFR3, and PDGFRβ did not significantly increase the loss of tumor blood vessels, pericytes, or lymphatic vessels caused by DC101 alone. Nevertheless, adding sunitinib to DC101, an antibody that specifically targets murine VEGFR2 [52], reduced the tumor volume to a greater extent than DC101 alone in one model (SKRC-29). This suggests that the multiple kinases inhibited by sunitinib on tumor and nontumor cells may still contribute toward tumor growth in ways separate from stroma-related mechanisms and distinct from the mechanistic targets of VEGFR2 antibody therapy. These distinct mechanisms will likely be of most value in designing novel combination approaches.

Acknowledgments

The authors thank Rajiv Bassi for his expert technical and administrative assistance, Keren Paz for oversight of the *vHL* sequencing work, and Kris Persaud for DC101 production.

References

[1] Matsumoto T and Claesson-Welsh L (2001). VEGF receptor signal transduction. *Sci STKE* **112**, 1–17.

[2] Hicklin DJ and Ellis LM (2005). Role of the vascular endothelial growth factor pathway in tumor growth and angiogenesis. *J Clin Oncol* **5**, 1011–1027.

[3] He Y, Rajantie L, Pajusola K, Jeltsch M, Holopainen T, Yla-Herttuala S, Harding T, Jooss K, Takahashi T, and Alitalo K (2005). Vascular endothelial cell growth factor receptor 3–mediated activation of lymphatic endothelium is crucial for tumor cell entry and spread via lymphatic vessels. *Cancer Res* **65**, 4739–4746.

[4] Casanovas O, Hicklin D, Bergers G, and Hanahan D (2005). Drug resistance by evasion of antiangiogenic targeting of VEGF signaling in late-stage pancreatic islet tumors. *Cancer Cell* **8**, 299–309.

[5] Folkman J, Merler E, Abemathy C, and Williams G (1971). Isolation of a tumor factor responsible for angiogenesis. *J Exp Med* **2**, 275–288.

[6] Hurwitz H, Fehrenbacher L, Novotny W, Cartwright T, Hainsworth J, Heim W, Berlin J, Baron A, Griffing S, Holmgren E, et al. (2004). Bevacizumab plus irinotecan, fluorouracil, and leucovorin for metastatic colorectal cancer. *N Engl J Med* **23**, 3697–3705.

[7] Kabbinavar FF, Schulz J, McCleod M, Patel T, Hamm JT, Hecht JR, Mass R, Perrou B, Nelson B, and Novotny WF (2005). Addition of bevacizumab to bolus fluorouracil and leucovorin in first-line metastatic colorectal cancer: results of a randomized phase II trial. *J Clin Oncol* **23**, 3697–3705.

[8] Johnson DH, Fehrenbacher L, Novotny WF, Herbst RS, Nemunaitis JJ, Jablons DM, Langer CJ, DeVore RF III, Gaudreault J, Damico LA, et al. (2004). Randomized phase II trial comparing bevacizumab plus carboplatin and paclitaxel alone in previously untreated locally advanced or metastatic non–small cell lung cancer. *J Clin Oncol* **22**, 2184–2191.

[9] Yang JC, Haworth L, Sherry RM, Hwu P, Schwartzentruber DJ, Topalian SL, Steinberg SM, Chen HX, and Rosenberg SA (2003). A randomized trial of bevacizumab, an anti–vascular endothelial growth factor antibody, for metastatic renal cancer. *N Engl J Med* **349**, 427–434.

[10] Miller KD, Chap LI, Holmes FA, Cobleigh MA, Marcom PK, Fehrenbacher L, Dickler M, Overmoyer BA, Reimann JD, Sing AP, et al. (2005). Randomized phase III trial of capecitabine compared with bevacizumab plus capecitabine in patients with previously treated metastatic breast cancer. *J Clin Oncol* **23**, 792–799.

[11] Gasparini G, Longo R, Fanelli M, and Teicher BA (2005). Combination of antiangiogenic therapy with other anticancer therapies: results, challenges, and open questions. *J Clin Oncol* **23**, 1295–1311.

[12] Tonra JR and Hicklin DJ (2007). Targeting the vascular endothelial growth factor pathway in the treatment of human malignancy. *Immunol Invest* **36**, 3–23.

[13] Jain RK (2005). Normalization of tumor vasculature: an emerging concept in antiangiogenic therapy. *Science* **307**, 58–62.

[14] Bergers G, Song S, Meyer-Morse N, Bergsland E, and Hanahan D (2003). Benefits of targeting both pericytes and endothelial cells in the tumor vasculature with kinase inhibitors. *J Clin Invest* **111**, 1287–1295.

[15] Willett CG, Boucher Y, di Tomaso E, Duda DG, Munn LI, Tong RT, Chung DC, Sahani DV, Kalva SP, Kozin SV, et al. (2004). Direct evidence that the VEGF-specific antibody bevacuzumab has antivascular effects in human rectal cancer. *Nat Med* **2**, 145–147.

[16] Dickson PV, Hamner JB, Sims TL, Fraga CH, Ng CYC, Rajasekeran S, Hagedorn NL, McCarville MB, Stewart CF, and Davidoff AM (2007). Bevacizumab-induced transient remodeling of the vasculature in neuroblastoma xenografts results in improved delivery and efficacy of systemically administered chemotherapy. *Clin Cancer Res* **13**, 3942–3950.

[17] Zhou Q, Guo P, and Gallo JM (2008). Impact of angiogenesis inhibition by sunitinib on tumor distribution of temozolomide. *Clin Cancer Res* **5**, 1540–1549.

[18] Winkler F, Kozin SV, Tong RT, Chae S-S, Booth MF, Garkavtsev I, Xu L, Hicklin DJ, Fukumura D, di Tomaso E, et al. (2004). Kinetics of vascular normalization by VEGFR2 blockade governs brain tumor response to radiation: role of oxygenation, angiopoetin-1, and matrix metalloproteinases. *Cancer Cell* **6**, 553–563.

[19] Inai T, Mancuso M, Hashizume H, Baffert F, Haskell A, Baluk P, Hu-Lowe DD, Shalinsky DR, Thurston G, Yancopoulos GD, et al. (2004). Inhibition of vascular endothelial growth factor (VEGF) signaling in cancer causes loss of endothelial fenestrations, regression of tumor vessels, and appearance of basement membrane ghosts. *Am J Pathol* **165**, 35–52.

[20] Tonra JR, Deevi DS, Corcoran E, Li H, Wang S, Carrick FE, and Hicklin DJ (2006). Synergistic antitumor effects of combined epidermal growth factor receptor and vascular endothelial growth factor receptor-2 targeted therapy. *Clin Cancer Res* **7**, 2197–2207.

[21] Shen J, Vil MD, Zhang H, Tonra JR, Rong LL, Damoci C, Prewett M, Deevi DS, Kearney J, Surguladze D, et al. (2007). An antibody directed against PDGF receptor β enhances the antitumor and the anti-angiogenic activities of an anti VEGF receptor 2 antibody. *Biochem Biophys Res Comm* **357**, 1142–1147.

[22] Shaheen RM, Tseng WW, Davis DW, Liu W, Reinmuth N, Vellagas R, Wieczorek AA, Ogura Y, McConkey DJ, Drazan KE, et al. (2001). Tyrosine kinase inhibition of multiple angiogenic growth factor receptors improves survival in mice bearing colon cancer metastases by inhibition of endothelial cell survival mechanisms. *Cancer Res* **61**, 1464–1468.

[23] Potapova O, Laird AD, Nannini MA, Barone A, Li G, Moss KG, Cherrington JM, and Mendel DB (2006). Contribution of individual targets to the antitumor efficacy of the multitargeted receptor tyrosine kinase inhibitor SU11248. *Mol Cancer Ther* **5**, 1280–1289.

[24] Guo P, Hu B, Gu W, Xu L, Wang D, Huang H-JS, Cavenee WK, and Cheng S-Y (2003). Platelet-derived growth factor-B enhances glioma angiogenesis by stimulating vascular endothelial growth factor expression in tumor endothelia and by promoting pericyte recruitment. *Am J Pathol* **162**, 1083–1093.

[25] Hellstrom M, Gerhardt H, Kalen M, Li X, Eriksson U, Wolburg H, and Betsholtz C (2001). Lack of pericytes leads to endothelial hyperplasia and abnormal vascular morphogenesis. *J Cell Biol* **153**, 543–553.

[26] Hirschi KK and D'Amore PA (1996). Pericytes in the microvasculature. *Cardio Res* **32**, 687–698.

[27] Mendel DB, Laird AD, Xin X, Louie SG, Christensen JG, Li G, Schreck RE, Abrams TJ, Ngai TJ, and Lee LB (2003). *In vivo* antitumor activity of SU11248, a novel tyrosine kinase inhibitor targeting vascular endothelial growth factor and platelet-derived growth factor receptors: determination of a pharmacokinetic/pharmacodynamic relationship. *Clin Cancer Res* **9**, 327–337.

[28] Cao R, Xue Y, Hedlund E-M, Zhong Z, Tritsaris K, Tondelli B, Lucchini F, Zhu Z, Dissing S, and Cao Y (2010). VEGFR1-mediated pericyte ablation links VEGF and PlGF to cancer-associated retinopathy. *Proc Natl Acad Sci USA* **107**, 856–861.

[29] Motzer RJ, Michaelson MD, Rosenberg J, Bukowski RM, Curti BD, George DJ, Hudes GR, Redman BG, Margolin KA, and Wilding G (2007). Sunitinib efficacy against advanced renal cell carcinoma. *J Urol* **178**, 1883–1887.

[30] Gnarra JR, Tory K, Weng Y, Schmidt L, Wei MH, Li H, Latif F, Liu S, Chen F, Duh FM, et al. (1994). Mutations of the *VHL* tumor suppressor gene in renal carcinoma. *Nat Genet* **1**, 85–90.

[31] Bottaro DP and Linehan WM (2005). Multifocal renal cancer: genetic basis and its medical relevance. *Clin Cancer Res* **20**, 7206–7208.

[32] Thompson CJ, Hoyle M, Green C, Liu Z, Weich K, Moxham T, and Stein K (2010). Bevacizumab, sorafenib tosylate, sunitinib and temsirolimus for renal cell carcinoma: a systematic review and economic evaluation. *Health Technol Assess* **2**, 1–184.

[33] Vaupel P (2004). The role of hypoxia-induced factors in tumor progression. *Oncologist* **9**, 10–17.

[34] Motzer RJ, Hutson TE, Tomczak P, Michaelson D, Bukowski RM, Rixe O, Oudard S, Negrier S, Szczylik C, Kim ST, et al. (2007). Sunitinib *versus* interferon α in metastatic renal-cell carcinoma. *N Engl J Med* **356**, 115–124.

[35] Bukowski RM, Kabbinavar FF, Figlin RA, Flaherty K, Srinivas S, Vaishampayan U, Drabkin HA, Dutcher J, Ryba S, Xia Q, et al. (2007). Randomized phase II study of erlotinib combined with bevacizumab compared with bevacizumab alone in metastatic renal cell cancer. *J Clin Oncol* **25**, 4536–4541.

[36] Agarwala SS and Case S (2010). Everolimus (RAD001) in the treatment of advanced renal cell carcinoma. *Oncologist* **15**, 236–245.

[37] Baffert F, Le T, Sennino B, Thurston G, Kuo CJ, Hu-Lowe D, and McDonald DM (2006). Cellular changes in normal blood capillaries undergoing regression after inhibition of VEGF signaling. *Am J Physiol Heart Circ Physiol* **290**, H547–H559.

[38] Kuhnert F, Tam BYY, Sennino B, Gray JT, Yuan J, Jocson A, Nayak NR, Mulligan RC, McDonald DM, and Kuo CJ (2008). Soluble receptor–mediated selective inhibition of VEGFR and PDGFRβ signaling during physiologic and tumor angiogenesis. *Proc Natl Acad Sci USA* **105**, 10185–10190.

[39] Yamagishi S, Yonekura H, Yamamoto Y, Fujimori H, Sakurai S, Tanaka N, and Yamamoto H (1999). Vascular endothelial growth factor acts as a pericyte mitogen under hypoxic conditions. *Lab Invest* **79**, 501–509.

[40] Sennino B, Kuhnert F, Tabruyn SP, Mancuso MR, Hu-Lowe DD, Kuo CJ, and McDonald DM (2009). Cellular source and amount of vascular endothelial growth factor and platelet-derived growth factor in tumors determine response to angiogenesis inhibitors. *Cancer Res* **69**, 4527–4536.

[41] Shibuya M and Claesson-Welsh L (2006). Signal transduction by VEGF receptors in regulation of angiogenesis and lymphangiogenesis. *Exp Cell Res* **312**, 549–560.

[42] Goldman G, Rutkowski JM, Shields JD, Pasquier MC, Cui Y, Schmokel HG, Willey S, Hicklin DJ, Pytowski B, and Swartz MA (2007). Cooperative and redundant roles of VEGFR-2 and VEGFR-3 signaling in adult lymphangiogenesis. *FASEB J* **21**, 1003–1012.

[43] Hong Y-K, Lange-Asschenfeldt B, Velasco P, Hirakawa S, Kunstfeld R, Brown LF, Bohlen P, Senger DR, and Detmar M (2004). VEGF-A promotes tissue repair–associated lymphatic vessel formation via VEGFR-2 and $\alpha_1\beta_1$ and $\alpha_2\beta_1$ integrins. *FASEB J* **10**, 1–21.

[44] Surguladze D, Steiner P, Prewett M, and Tonra JR (2010). Methods for evaluating effects of an irinotecan + 5-fluorouracil/leucovorin (IFL) regimen in an orthotopic metastatic colorectal cancer model utilizing *in vivo* bioluminescence imaging. *Methods Mol Biol* **602**, 235–252.

[45] Ebert T, Bander NH, Finstad CL, Ramsawak RD, and Old LJ (1990). Establishment and characterization of human renal cancer and normal kidney cell lines. *Cancer Res* **50**, 5531–5536.

[46] Tong RT, Boucher Y, Kozin SV, Winkler F, Hicklin DJ, and Jain RK (2004). Vascular normalization by vascular endothelial growth factor receptor 2 blockade induces a pressure gradient across the vasculature and improves drug penetration in tumors. *Cancer Res* **64**, 3731–3736.

[47] Tonra JR, Corcoran E, Deevi DS, Steiner P, Kearney J, Li H, Ludwig DL, Zhu Z, Witte L, Surguladze D, et al. (2009). Prioritization of EGFR/IGF-1R/VEGFR2 combination targeted therapies utilizing cancer models. *Anticancer Res* **29**, 1999–2009.

[48] Boucher Y, Baxter LT, and Jain RK (1990). Interstitial pressure gradients in tissue-isolated and subcutaneous tumors: implications for therapy. *Cancer Res* **50**, 4478–4484.

[49] Prewett M, Huber J, Li Y, Santiago A, O'Connor W, King K, Overholser J, Hooper A, Pytowski B, Bohlen P, et al. (1999). Antivascular endothelial growth factor receptor (fetal liver kinase 1) monoclonal antibody inhibits tumor angiogenesis and growth of several mouse and human tumors. *Cancer Res* **59**, 5209–5218.

[50] Liang W-C, Wu X, Peale FV, Lee CV, Meng YG, Gutierrez J, Fu L, Malik AK, Gerber H-P, Ferrara N, et al. (2006). Cross-species vascular endothelial growth factor (VEGF)–blocking antibodies completely inhibit the growth of human tumor xenografts and measure the combination of stromal VEGF. *J Biol Chem* **281**, 951–961.

[51] Huang D, Ding Y, Li Y, Luo W-M, Zhang Z-F, Snider J, VandenBeldt K, Qian C-N, and Teh BT (2010). Sunitinib acts primarily on tumor endothelium rather than tumor cells to inhibit the growth of renal cell carcinoma. *Cancer Res* **70**, 1053–1062.

[52] Witte L, Hicklin DJ, Zhu Z, Pytowski B, Kotanides H, Rockwell P, and Bohlen P (1998). Monoclonal antibodies targeting VEGF receptor-2 (Flk1/KDR) as an anti-angiogenic therapeutic strategy. *Cancer Metastasis Rev* **17**, 155–161.